Liquid Crystals
Publication details, including instructions for authors and subscription information:
http://www.informaworld.com/smpp/title~content=t713926090

S_{C^*A} and S* phases in chiral non-symmetric dimesogens

V. Faye[a]; A. Babeau[a]; F. Placin[a]; H. T. Nguyen[a]; P. Barois[a]; V. Laux[b]; N. Isaert[b]
[a] Centre de Recherche Paul Pascal, Pessac, France [b] Laboratoire de Structure et Dynamique des Matériaux Moléculaires, Université de Lille I, Villeneuve d'Ascq, France

To cite this Article Faye, V. , Babeau, A. , Placin, F. , Nguyen, H. T. , Barois, P. , Laux, V. and Isaert, N.(1996) 'S_{C^*A} and S* phases in chiral non-symmetric dimesogens', Liquid Crystals, 21: 4, 485 — 503
To link to this Article: DOI: 10.1080/02678299608032857
URL: http://dx.doi.org/10.1080/02678299608032857

LIQUID CRYSTALS, 1996, VOL. 21, NO. 4, 485–503

S_{C*A} and $S_{\tilde{C}*}$ phases in chiral non-symmetric dimesogens

by V. FAYE, A. BABEAU, F. PLACIN, H. T. NGUYEN*, P. BAROIS, V. LAUX†, and N. ISAERT†

Centre de Recherche Paul Pascal, Av. A. Schweitzer, 33600 Pessac, France,
†Laboratoire de Structure et Dynamique des Matériaux Moléculaires, Université de Lille I, 59655 Villeneuve d'Ascq, France

(*Received 3 April 1996; accepted 14 June 1996*)

We have synthesized two separate homologous series of chiral non-symmetric dimesogens: these have a two phenyl ring moiety bearing a terminal alkoxy chain linked via a methylenic spacer to a chiral three phenyl ring mesogen which itself displays antiferroelectric properties. Depending on the parity of the number of carbons constituting the spacer, two kinds of mesomorphic behaviour have been found. When the spacer is even, various S_{C*} phases (S_{C*A}, S_{C*Fl}, S_{C*}, $S_{C*\alpha}$) have been identified without doubt, whereas when the spacer is odd, a tilted modulated phase ($S_{\tilde{C}*}$) has been observed and characterized. In each case, we study the effect of the length of the alkoxy chain at the end of the shorter moiety. The alternation of the mesomorphic behaviour with the spacer parity has been interpreted in terms of molecular shape, but we have also discussed the influence of some chemical parameters on the stability of the S_{C*A} phase.

1. Introduction

Up to now, most low molar mass liquid crystals involved molecules constituting one single rigid core and one or two aliphatic parts, leading to a rod-like shape. A few years ago, a new interest in the study of twin liquid crystals emerged, stimulated by research on models for semi-flexible main chain [1] and also side chain [2] liquid crystalline polymers. Most of the dimeric compounds, also called 'twins', which have been investigated so far contain two identical mesogenic units (see, for example [3]).

More recently, a new architecture has been introduced, consisting of two different mesogenic units linked via a flexible spacer [4]. These three-block molecules give rise to very interesting smectic phases: intercalated and interdigitated smectic phases in the case of a polar mesogen linked to a non-polar mesogen [5], and an incommensurate S_A phase for a compound having a cholesteryl group [6].

One of the most striking features of the dimesogenic compounds is the strong role played by the number of flexible units in the spacer, especially on the clearing temperatures and their associated entropies [7]. Concerning non-symmetric dimesogens, the spacer length induces modifications in the structure of the smectic phases [8, 9]. The terminal chain length is also an important parameter in both symmetric [10] and non-symmetric systems [5].

Within the framework of our programme of synthesis of new antiferroelectric liquid crystals (AFLCs), it seemed to be interesting to attach one of our low molar mass AFLC compounds to a non-chiral mesogen having a different length. We had already demonstrated the antiferroelectric behaviour of two chiral non-symmetric dimesogens [11], and had carried out several experiments in order to characterize beyond doubt the S_{C*A} phase. Note that, a simple miscibility test with a reference AFLC compound was not possible because of a large difference in smectic layer spacings.

In this paper, we study the influence of the spacer length (n) and the alkoxy chain length (m) at the non-chiral end, in two series of related compounds:

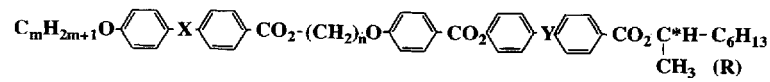

where X = Y = CO_2: series mBBnBBB8*; or where X = Y = –(single bond): series mBPnBBP8*.

As in the previous work [11], the three phenyl ring chiral mesogens themselves exhibit antiferroelectric behaviour [12, 13].

*Author for correspondence.

0267–8292/96 $12·00

2. Experimental

2.1. *Synthesis*

2.1.1. *Synthesis of mBBnBBB8**

The synthetic route is briefly summarized below:

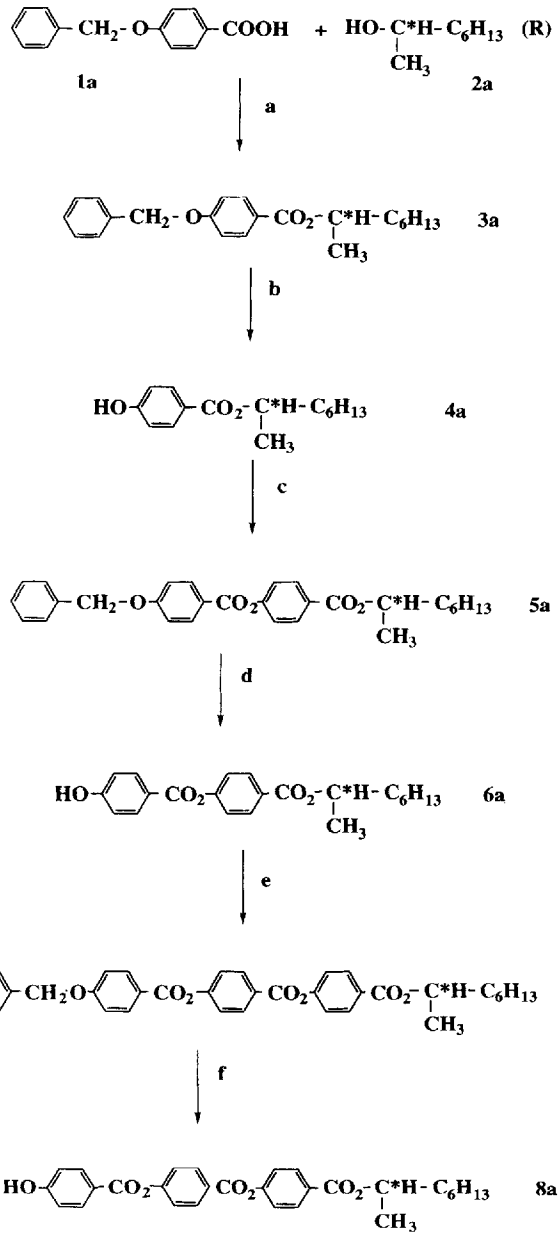

a: DCC, DMAP, CH_2Cl_2; b: H_2, Pd/C, AcOEt, EtOH (95%); c: **1a**, DCC, DMAP, CH_2Cl_2; d: H_2, Pd/C, AcOEt, EtOH (95%); e: **1a**, DCC, DMAP, CH_2Cl_2; f: H_2, Pd/C, AcOEt, EtOH (95%).

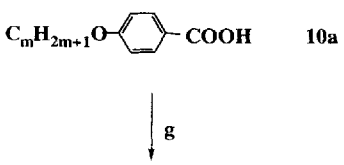

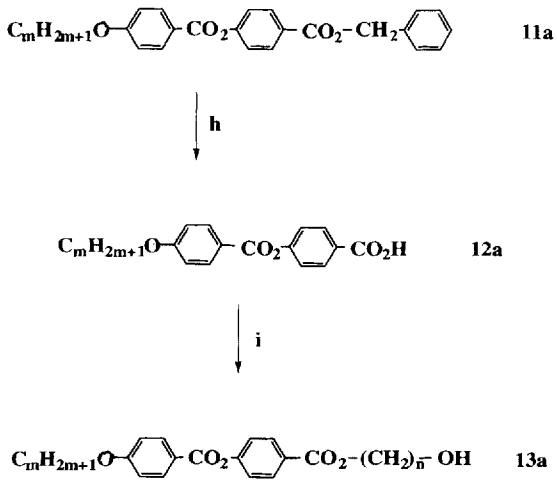

g: 4-HOPhCO$_2$CH$_2$Ph, DCC, DMAP, CH_2Cl_2; h: H_2, Pd/C, AcOEt, EtOH (95%); i: HO–$(CH_2)_n$–OH, DCC, DMAP, CH_2Cl_2.

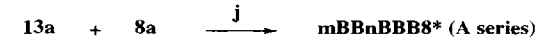

j: TPP, DEAD, CH_2Cl_2.

The synthesis of the two phenyl ring chiral phenol **6a** has been described previously [13]. The three phenyl ring chiral phenol is obtained by a further esterification and hydrogenolysis.

The carboxylic acids **12a** were prepared following a well-known method. A two phenyl ring acid is obtained by an esterification reaction with benzyl 4-hydroxybenzoate, followed by hydrogenolysis. An esterification reaction using a large excess of alkan-1, ω-diol leads to the shorter non-chiral mesogen. This latter compound and the chiral phenol form the final dimesogen via an etherification reaction using triphenylphosphine (TPP) and diethyl azodicarboxylate (DEAD).

2.1.2. *Synthesis of mBPnBBP8**

The synthetic route is briefly summarized below:

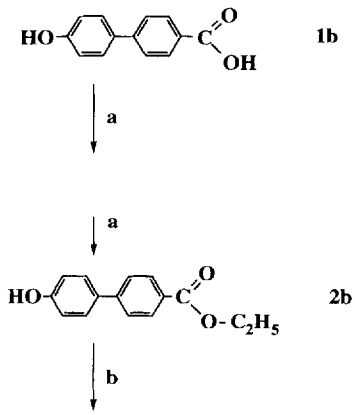

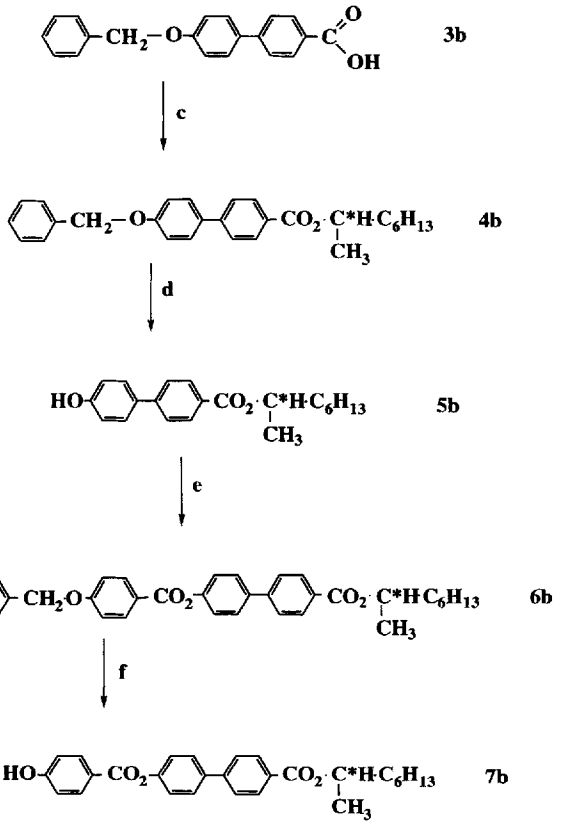

a: H_2SO_4, EtOH; b: 1.$PhCH_2Br$, KOH, EtOH, 2. KOH, 3. HCl; c: 1. $(COCl)_2$, 2. (*R*)-2-octanol, pyridine, 3. HCl; d: H_2, Pd/C, AcOEt, EtOH (95%); e: **1a**, DCC, DMAP, CH_2Cl_2; f: H_2, Pd/C, AcOEt, EtOH (95%).

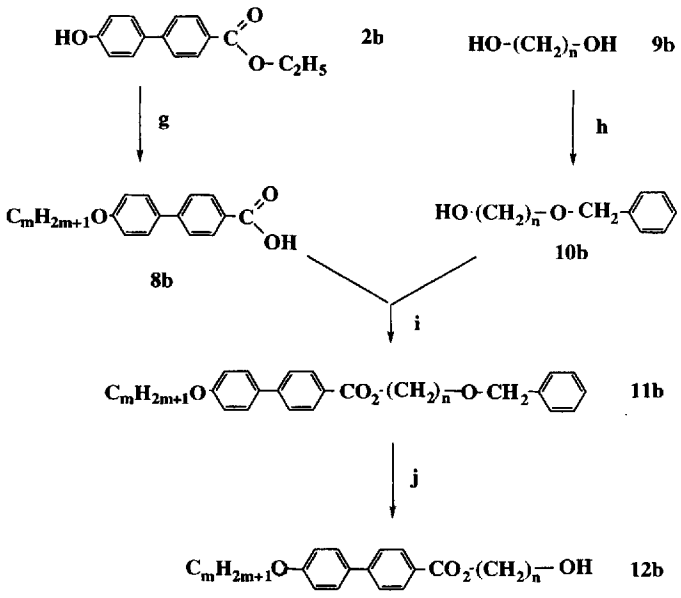

g: 1. $C_mH_{2m+1}Br$, EtOH, KOH, 2. KOH, 3. HCl; h: 1. Na, toluene, 2. $PhCH_2Br$, 3. HCl; i: DCC, DMAP, CH_2Cl_2; j: $Pd(OH)_2$, cyclohexene.

k: TPP, DEAD, CH_2Cl_2.

This synthetic route is also divided into two main parts: the synthesis of the three phenyl ring chiral phenol on the one hand, and the synthesis of the two phenyl ring alcohols on the other hand; these are then linked together via an etherification reaction using TPP and DEAD.

2.2. *Characterization*

2.2.1. *Chemical characterization*

The purity of all intermediate and final compounds was checked by thin layer chromatography (using Merck plastic sheets, silica gel 60). Their chemical structures were confirmed by ^1H NMR (Bruker Am200) and by Fourier transform infra red spectroscopy (Nicolet MX-1). The purity of the final products was checked by normal phase HPLC using a Waters 600E system controller. Chromatography was carried out on silical gel (Waters Microporasil 10 μm particle size) using CH_2Cl_2 as eluent. Detection of the eluting products was achieved using a Waters 484 UV-VIS detector ($\lambda = 254$ nm). Each of the final products was found to have a purity exceeding 99 per cent.

2.2.2. *Mesomorphic properties*

The thermal behaviour of the mesogens was investigated by differential scanning calorimetry (Perkin-Elmer DSC7) and the first step in phase identification was carried out by thermal optical microscopy, using a Zeiss Ortholux polarizing microscope equipped with a Mettler FP5 hot stage. The transition temperatures and their associated entropies are reported in tables 1, 2, 3, 4.

In order to confirm the nature of the phases exhibited, it was often necessary to use several methods of characterization such as X-Ray diffraction and measurements of helical pitch or electro-optic properties.

X-Ray diffraction was performed as follows. The CuKα radiation from an 18 kW rotating anode X-ray generator (Rigaku-200) was selected by a flat pyrolitic graphite (002) monochromator, which delivers a 1 mm^2 beam onto the sample. The scattered radiation was collected on a two dimensional detector (Imaging Plate system purchased from Mar Research, Hamburg). The sample to detector distance was 1180 mm through helium, in order to lower absorption and diffusion. Then, the instrumental resolution was about $1{\cdot}5 \times 10^{-2}$ $Å^{-1}$ (FWHM). A flat (111) germanium monochromator was also used whenever better collimation was necessary. Under such conditions, the instrumental resolution was about 7×10^{-3} $Å^{-1}$, with a sample to detector distance of 830 mm. In both cases, Lindemann tubes ($\Phi = 1$ mm) were filled by capillarity from the isotropic phase without

any alignment procedure. They were placed in an oven, the temperature of which was controlled within ± 10 mK. The tube axis was vertical and perpendicular to the beam. Exposure times were 30 min.

Helical pitch measurements were made in the following way. For the S_{C*} and S_{C*A} phases, we used a well-known method, as previously described [14, 15]: a prismatic cell made of rubbed glass plates contained the liquid crystal which adopts a planar orientation and presents a lattice of regular Grandjean-Cano steps. For the $S_{C*\alpha}$ phase, the preparation of a very thin pseudo-homeotropic drop allowed the observation of fringes resulting from the variations in ellipticity of the propagating light [16].

Electric field dependent properties were investigated using commercial cells (from E.H.C.) coated with indium-tin oxide over a 0·16 cm^2 active area. The inner surfaces were covered with a uni-directionally rubbed polyimide layer. The thickness of the cells was 3 μm. A classical electro-optical set-up was used for the measurements of switching current and apparent tilt angle [17].

3. Results

3.1. *Phase assignment*

The observed type of texture depends on the parity of the spacer. Therefore, we will describe two cases. At this stage, it is worth noticing that the parity of the number of carbons in the spacer differs from that of the number of methylene units due to the presence of the carboxy group linking the first mesogenic moiety and the spacer.

3.1.1. *n is odd*

We choose to describe with accuracy the mesomorphic behaviour of one compound in each series.

*10BB5BBB8**. The DSC trace exhibits peaks at 142, 152 and 184°C. On cooling from the isotropic liquid, some coloured stripes appear, which grow and curl up in order to form focal-conic fan defects. Moreover, the presence of homeotropic domains is typical of an S_A phase. On further cooling, no textural change can be observed until 142°C, when the focal-conic fan texture becomes broken and striated, with rather dark pseudo-homeotropic domains, indicating the transition to an S_{C*} phase. The presence of an $S_{C*\alpha}$ phase between the S_A and the S_{C*} phases was expected, but even a good planar alignment gave no indication of this.

Only the observation of free droplets, with planar alignment, allowed us to visualize the $S_{C*\alpha}$ phase [16]. The mobile Friedel fringes were visible over a large temperature range, and gave an estimation of the helical pitch. The $S_{C*\alpha}$ phase persists over 6·8°C on heating, and over 3·5°C on cooling. Its pitch is short, about 0·18 μm, except close to the S_A phase, where it reaches 0·36 μm.

In the S_{C*} phase, the helical pitch was measured in the prismatic cell, with a planar alignment. In this cell, the S_{C*} phase occurs from 117·9 to 135·2°C (under these conditions, we note an important undercooling effect). The helical pitch is about 0·59 μm from 119 to 134°C, and decreases to 0·53 μm at 134·4°C, and to 0·4 μm at 134·9°C (figure 1). The sample is colourless with orange Grandjean–Cano threads from 117·9 to 134°C and becomes orange just before the high temperature transition, corroborating the pitch measurements. In the S_{C*} phase, at low temperature, the Grandjean–Cano threads are single. On heating, 2°C before the high temperature transition, they split up into parallel lines. This phenomenon generally precedes an S_{C*}–S_{C*FI} transition (see the 12BP5BBP8* compound, where it occurs on cooling). An S_{C*FI} phase can be expected between S_{C*} and $S_{C*\alpha}$ phases. Nevertheless, this S_{C*FI} does not appear in a prismatic cell; on a free droplet, it seems to occur over a narrow temperature domain, and to be stable only if the temperature changes very slowly (see figure 2, in which the region striated with many defects could be an S_{C*FI} phase).

X-ray diffraction experiments were also carried out. In the S_A phase, the intensity profile shows two Bragg reflection peaks (first and second order) in the low angle region at $q_0 = 0{\cdot}111$ Å^{-1} and $2q_0 = 0{\cdot}222$ Å^{-1}. The corresponding layer periodicity is 56·4 Å. As the temperature decreases (see figure 3), the periodicity remains quasi-constant over the S_A temperature range, but decreases from 150 to 142°C where it reaches another plateau. This variation can be interpreted as a progressive tilt of the director from the layer normal, confirming the existence of a tilted smectic phase between the S_A and the S_{C*} phases. In the S_{C*} phase, the calculated angle ($\cos\Theta = d_{SC*}/d_{SA}$) is about 10 degrees.

The molecular length was calculated considering the molecule in the all-*trans*-conformation and assuming that the chiral chain lies perpendicular to the long axis of the molecule. This position of the chiral chain has been supported by several structural investigations of the crystalline state [18, 19]. It has also been suggested in the liquid crystalline state: lengthening of the chiral ramification leads to an increase in the smectic spacing, indicating that this lateral substituent lies along the molecular long axis [20]. In our estimation of the molecular length, the contribution of the chiral part corresponds to its projection on the long axis. In the S_A phase, the layer spacing corresponds to the length of a single molecule ($l = 58$ Å). This result is consistent with results obtained for dimesogenic tolane compounds [11].

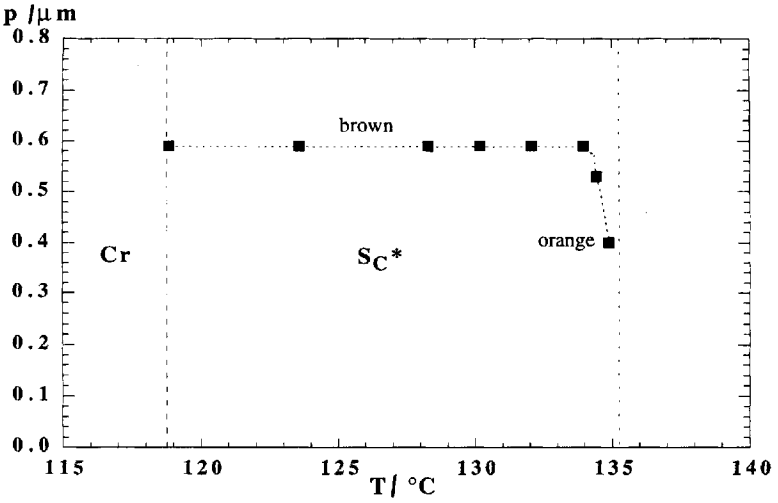

Figure 1. Helical pitch versus temperature for the S_{C*} phase of 10BB5BBB8*. The high temperature transition of the S_{C*} phase corresponds to the disappearance of the Grandjean–Cano defects in a prismatic cell.

In summary, the compound **10BB5BBB8*** exhibits the sequence: Cr–S_{C*}–$S_{C*\alpha}$–S_A–I.

The study of the rest of the series *m*BB*n*BBB8* with an odd value of *n* involves no other phase, except for $m=9$, where a new phase appears at low temperatures, just before recrystallization occurs. In the pseudo-homeotropic domain, its texture consists of constantly moving grey defects typical of an S_{C*FI} phase. However, its monotropic nature prevented us from making any physical characterization.

Tables 1 and 2 summarize the transition temperatures and their associated entropy changes.

*12BP5BBP8**. The second series displays a richer polymorphism. For example, the 12BP5BBP8* compound behaves like 10BB5BBB8* at high temperatures, with the same order of magnitude for the clearing temperature (181°C) and the appearance of the striated focal-conic fan defects of the S_{C*} phase at 164°C (the $S_{C*\alpha}$ is probably present, but is not detected by DSC). On cooling from the S_{C*} phase, at 100°C the typical texture of an S_{C*FI} phase is briefly observed, immediately followed by a texture similar to the S_{C*} phase, which could be an S_{C*A} phase.

Because of the short enantiotropic temperature range of existence of this latter phase, evidence for the tristable switching behaviour under an a.c. field could not be obtained using a thin cell (3 μm). As for the homologous 10B5T8* tolane [11] (to maintain our notation, it should have the abbreviation 10BP5TBB8*), the surface anchoring effect is strong enough to shift the S_{C*}–S_{C*A} transition temperature below that of recrystallization. Therefore, this compound only exhibits ferroelectric behaviour in a thin cell. Using a thicker cell did not solve the problem, since it was not possible to get a good uni-directional alignment. However, the spontaneous polarization (figure 4) under saturation conditions (in the ferroelectric state) and the apparent tilt angle (figure 5) have been measured at various temperatures

Table 1. Transition temperatures (°C) and associated entropies ($\Delta S/R$) (in italics) resulting from DSC measurements and optical observations on the 10BB*n*BBB8* series.

m	*n*	Cr	$S_{\tilde{C}*}$	S_{C*}	$S_{C*\alpha}$	S_A	I
10	3	• 154 *17·5*	—	• 190 *?*	• 201 *0·02*	• 211 *4·2*	•
10	4	• 120 *13·8*	• 140 *4·4*	—		—	•
10	5	• 136 *16·0*	—	• 142 *0·002*	• 152 *0·011*	• 184·5 *4·2*	•
10	6	• 113 *13·8*	• 132 *4·8*	—	—	—	•
10	7	• 143·5 *18·5*	—	—	—	• 159 *4·3*	•
10	8	• 103 *13·6*	• 124 *4·7*	—	—	—	•
10	9	• 143 *20·5*	—	—		• 143 *4·0*	•

Table 2. Transition temperatures (°C) and associated entropies ($\Delta S/R$) (in italics) resulting from DSC measurements and optical observations on the *m*BB5BBB8* series. ( ) denotes a monotropic transition; # is the sum of S_{C*}–$S_{C*\alpha}$ and $S_{C*\alpha}$–S_A entropies. The existence of an $S_{C*\alpha}$ phase is not always detected simply by using optical microscopy or DSC.

m	*n*	Cr	S_{C*FI}	S_{C*}	$S_{C*\alpha}$	S_A	I
9	5	• 148 *17·8*	• (121·6) ?	• (128·8) *0·001*	• (141·2) *0·012*	• 185·5 *4·16*	•
10	5	• 136 *16*	—	• 142 *0·002*	• 152 *0·011*	• 184 *4·06*	•
11	5	• 122 *19*	—	• 150 *0·020*	• ?	• 181 *4·02*	•
12	5	• 120 *15·9*	—	• 159	• 163 *0·027#*	• 183 *4·16*	•
13	5	• 117 *17·2*	–	• 164 *0·055*	—	• 181 *4·13*	•
14	5	• 115 *18·8*	—	• 168 *0·040*	–	• 180 *4·3*	•
15	5	• 113 *18·8*	—	• 171 *0·050*	–	• 180 *4·31*	•
16	5	• 113 *18·8*	—	• 171 *0·057*	–	• 180 *4·4*	•

($E = 2{\cdot}5\ V\ \mu m^{-1}$, $\nu = 50$ Hz for the polarization measurements, and $\nu = 0{\cdot}1$ Hz for the apparent tilt angle). Both curves show a regular decrease with temperature. The upper values are $80\ nC\ cm^{-2}$ for the polarization, and 35 degrees for the tilt angle, values of the same order of magnitude as for the dimesogenic tolanes [11].

In a prismatic cell, no Grandjean–Cano step forms in the S_{C*A} phase. For a free drop, the Grandjean–Cano threads seem to be twice as tight as in the S_{C*} phase; the pitch is in the same range for both phases (about 0·65 μm). In the S_{C*A} phase, the sample is brown with orange Grandjean–Cano threads, in keeping with this pitch value.

The S_{C*} phase occurs from 106 to 166·7°C. The pitch increases from 0·58 μm at 107°C to 0·67 μm at 163°C. It does not vary up to 165·5°C, and then falls, reaching 0·18 μm at 166·5°C (figure 6). From 107 to 165°C, the sample is brown, and colourless; from 165 to 165·5°C, second ($\lambda = np$) and first ($\lambda = 2np$) order selective reflection spectra are visible one after the other. This observation corroborates the pitch measurements. The Grandjean–Cano threads begin to split up into two parallel lines at 118°C on cooling, about 12°C before the S_{C*}–S_{C*FI} transition (figure 7). Near the phase transition, with a free drop, the texture looks like the superposition of two similar lattices, shifted by almost half a pitch. The S_{C*FI} phase was observed between 103 and 106°C on cooling.

The $S_{C*\alpha}$ phase was observed using a free droplet (figure 8). It occurs from 167 to 167·8°C on heating, and from 167·7 to 166·7°C on cooling. The pitch decreases to 0·18 μm on heating, and exhibits a divergence on cooling; its behaviour is represented in figure 9.

As for the 10BB5BBB8* benzoate ester, X-ray diffraction experiments give the layer spacing in the smectic phases as a function of temperature (figure 10). This is 53·1 Å over the S_A phase range, decreasing regularly from 165 to 110°C due to the tilt of the director from the layer normal and staying constant until recrystallization occurs at 95°C. This constant value of the periodicity is 49·2 Å and the calculated angle is equal to 22 degrees. Once again, the layer periodicity in the S_A phase corresponds to the length of one single molecule in the all-*trans*-conformation ($l = 55$ Å).

In addition, a miscibility test with a reference compound has been performed. The chosen reference compound was 10B5T8* [11] because it provides both the required characteristics—an S_{C*A} phase and a layer periodicity close to that of 12BP5BBP8*. The continuous miscibility across the whole composition range between the two (*R*)-enantiomers confirms their isomorphism. Other *m*BP*n*BBP8* (*n* is odd) compounds have been studied by optical microscopy and DSC. They display the same mesomorphic sequence, except for 10BP9BBP8* where no S_{C*A} phase has been observed (see table 3).

In this section, it has been shown that dimesogenic compounds with an odd number of methylene units in the spacer exhibit a mesomorphic behaviour including the sequence S_A–$S_{C*\alpha}$–S_{C*}. The *m*BP*n*BBP8* series displays additionally some S_{C*FI} and S_{C*A} phases. The usual different methods of investigation were performed to check their nature.

3.1.2. *n is even*

We now describe in detail the behaviour of the compound 16BB6BBB8*. Cooling down slowly from the isotropic phase, at 132°C large focal-conic defects begin

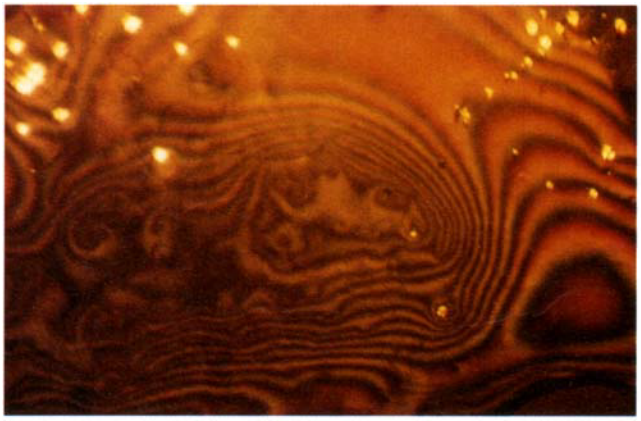

Figure 2. On this free drop, the domain with many defects may be an S_{C*FI} phase occurring between the S_{C*} and $S_{C*\alpha}$ phases in the 10BB5BBB8* sequence, when cooling very slowly. Here the temperature is 142·0°C; magnification × 350.

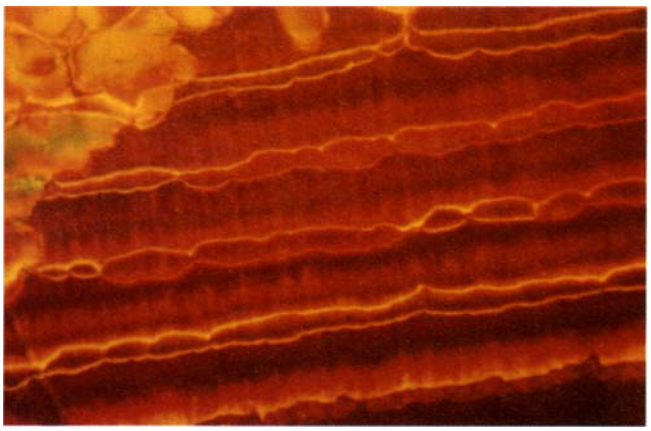

Figure 7. In the S_{C*} phase, Grandjean–Cano threads split up into two parallel lines when approaching the transition, on cooling. Here, for the 12BP5BBP8* compound, at 107·5°C, in a prismatic cell, just before the phase transition; magnification × 350.

to develop among homeotropic domains: this texture is characteristic of an S_A phase (figure 11(*a*)). At 127°C, a drastic change occurs, corresponding to a first-order transition ($\Delta S/R = 0{\cdot}9$). Focal-conic groups become crumpled and some grey defects (looking like small Maltese crosses) appear all over the homeotropic part (see figure 11(*b*)). This texture is not a classical one for chiral compounds, but reminds one of a texture previously observed in polar compounds: the $S_{\tilde{C}}$ phase [21].

Thanks to their ability to form antiparallel pairs, such materials can display particular smectic phases with a periodicity corresponding to the pair length [22]. Additionally, two fluid bidimensional phases are characterized by the in-plane modulation of the bilayer density wave: the $S_{\tilde{A}}$ (antiphase) [23] and the $S_{\tilde{C}}$ (ribbon phase)

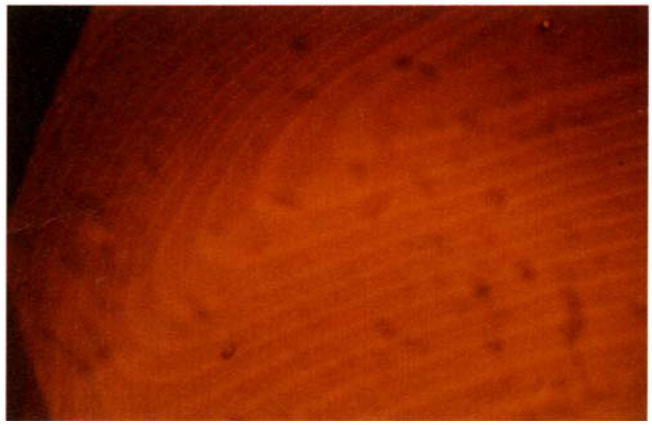

Figure 8. On a free drop, the $S_{C*\alpha}$ phase is characterized by many Friedel fringes. Here, for 12BP5BBP8*, at 167·6°C, magnification × 350.

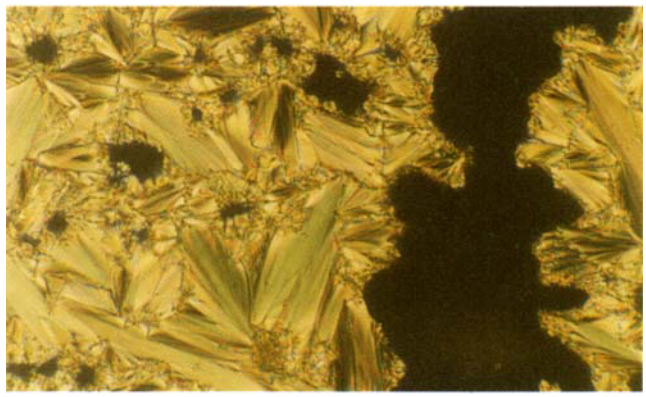

(*a*)

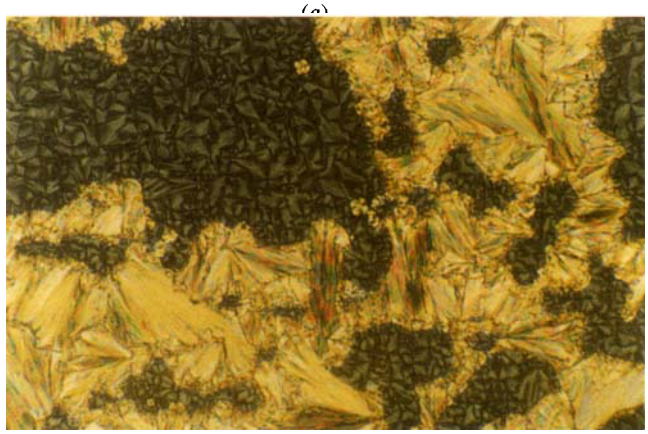

(*b*)

Figure 11. Optical texture of the S_A (*a*) and $S_{\tilde{C}*}$ (*b*) phases of 16BB6BBB8*; magnification × 350.

[21], which have, respectively, a centred rectangular and an oblique lattice (represented in figures 12 and 13). An anticipated X-ray diffraction pattern for an aligned sample of an $S_{\tilde{C}}$ phase is represented in figure 14.

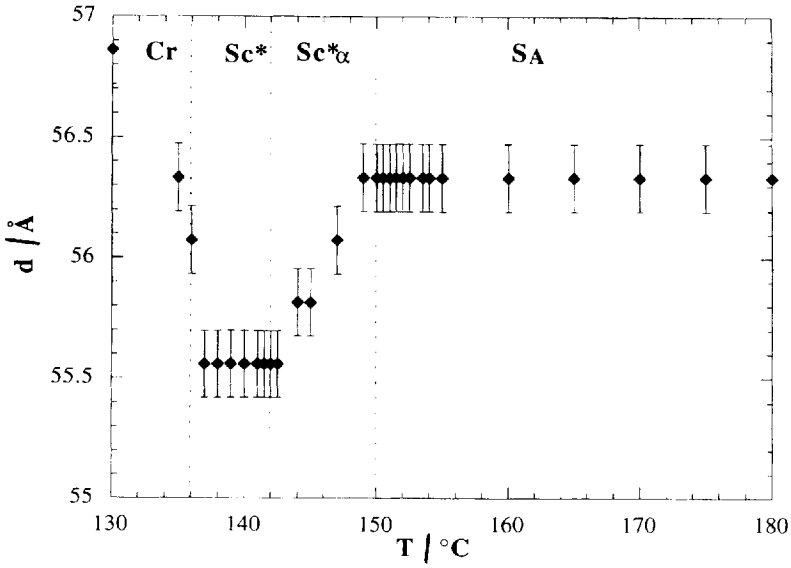

Figure 3. Temperature dependence of the layer spacing resulting from X-ray scans for 10BB5BBB8*, using a graphite monochromator (instrumental resolution: $1{\cdot}5 \times 10^{-2}$ Å^{-1}).

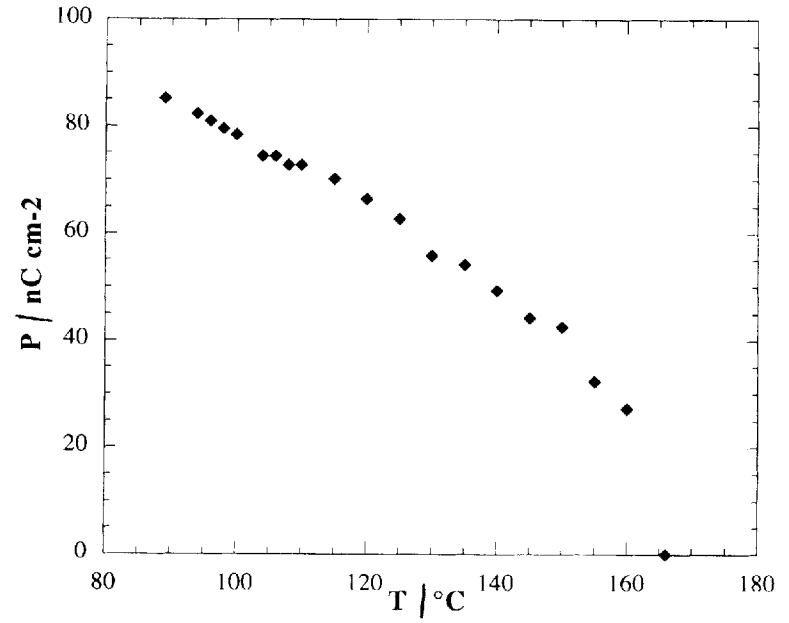

Figure 4. Temperature dependence of the polarization at saturation for 12BP5BBP8*; $E = 2{\cdot}5$ V μm^{-1}, $\nu = 50$ Hz.

In order to characterize this phase, we have carried out X-ray diffraction experiments on a powder sample of 16BB6BBB8*. As shown in figure 15, four wave vectors are detected in the small angle region: $q_1 = 0{\cdot}043$, $q_2 = 0{\cdot}111$, $q_3 = 0{\cdot}125$ and $q_4 = 0{\cdot}222$ Å^{-1}. The last one can be interpreted as the second harmonic of q_2. The three others do not index on a one-dimensional lattice.

A successful alignment procedure was performed as follows. Two thin glass plates (50 μm) were coated with polyimide and unidirectionally rubbed; the liquid crystal was introduced by capillarity in its isotropic phase, cooled down into the S_A phase and sheared following the rubbing direction. The X-ray diffraction pattern displayed two Bragg spots lying along the z-axis and corresponding to q_2. No other spot was observed, suggesting that those wave vectors lie out of the incident plane. Therefore, a rotation around the vertical axis of the sample was necessary. Unfortunately, our experimental apparatus allowed us rotation by only a few degrees and the other wave vectors were not observed. However, the combination of the two experimental techniques (powder X-ray diffraction and optical microscopy) confirms the idea of the presence of a two-dimensional phase such as $S_{\tilde{C}}$. The observed reflections (figure 15) correspond to 10, 01, 11, 02, respectively, and the calculated lattice parameters at 127°C are $a = 146$ Å

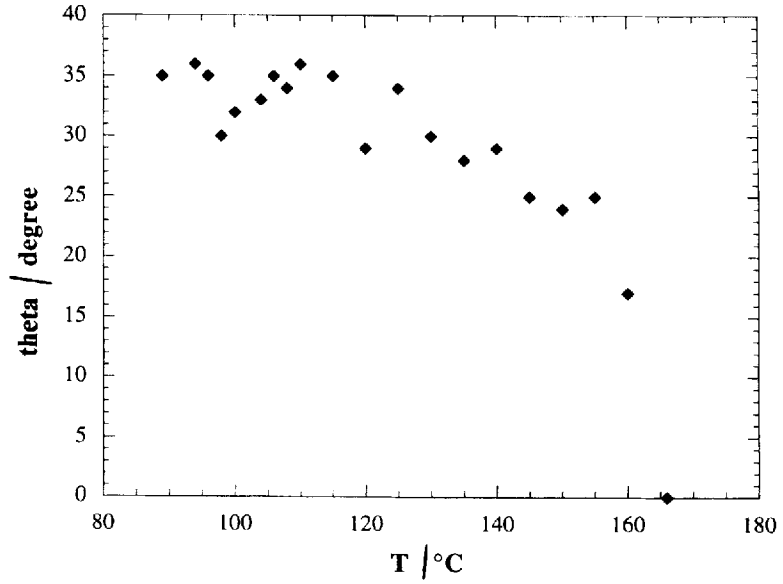

Figure 5. Temperature dependence of the apparent tilt angle at saturation for 12BP5BBP8*: $E=2{\cdot}5\,\mathrm{V\,\mu m^{-1}}$, $\nu=0{\cdot}1$ Hz.

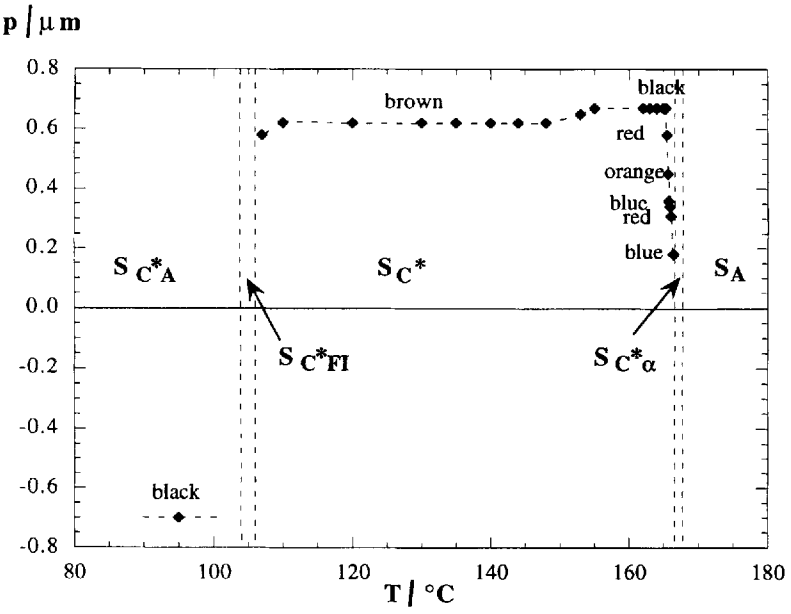

Figure 6. Helical pitch versus temperature and selective reflection colours for the S_{C*} and S_{C*A} phases of 12BP5BBP8*.

and $c=56{\cdot}6$ Å, the angle between the lattice vectors being $\gamma=108°$. These values are close to these found by Date *et al.* for an $S_{\tilde{C}}$ like phase with additional in-plane hexatic order [10, 24].

We have also checked the fluid character of this phase: the wide angle region exhibits a broad diffuse ring, centred at a spacing of 4·7 Å. Although the presence of a helix in this structure remains unconfirmed this phase will be referred to as $S_{\tilde{C}*}$, since any other tilted smectic phase of a chiral liquid crystal has always received the superscript asterisk.

In the S_A phase, the layer spacing is constant and equal to 56·6 Å, indicating a monolayer ordering. The smectic periodicity of 16BB6BBB8* is lower than that of 16BB5BBB8* (59·2 Å), in spite of its shorter alkyl spacer. This result suggests that, with the spacer in the all-*trans*-conformation, the dimesogens bearing an even number of carbons in the spacer can adopt a rod-like shape, whereas the odd ones are bent. Then, we could easily understand the decrease in the smectic spacing by increasing the molecular length by one carbon atom. The alternation of the mesomorphic behaviour between odd and even spacers is probably linked to the alternation of the molecular shape.

X-ray diffraction experiments have been carried out at various temperatures. In figure 16, the wave vectors

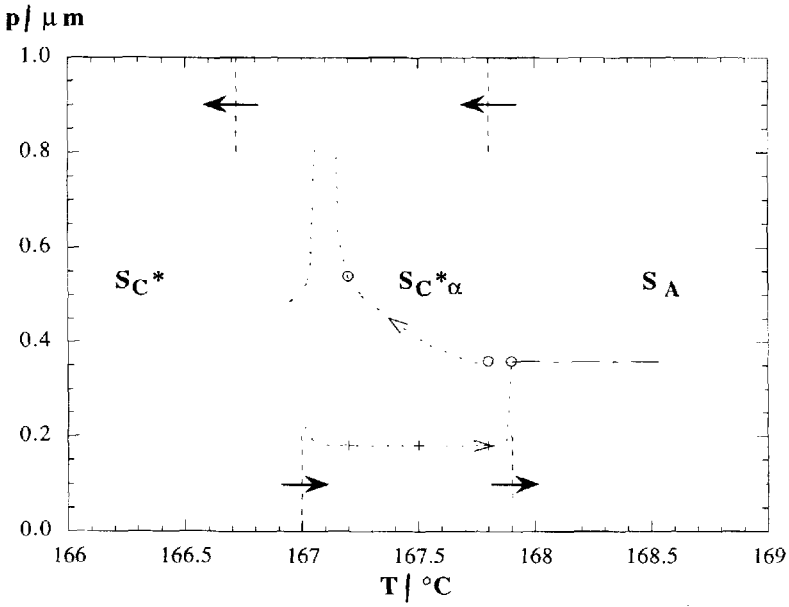

Figure 9. Helical pitch versus temperature for the $S_{C*\alpha}$ phase of 12BP5BBP8*.

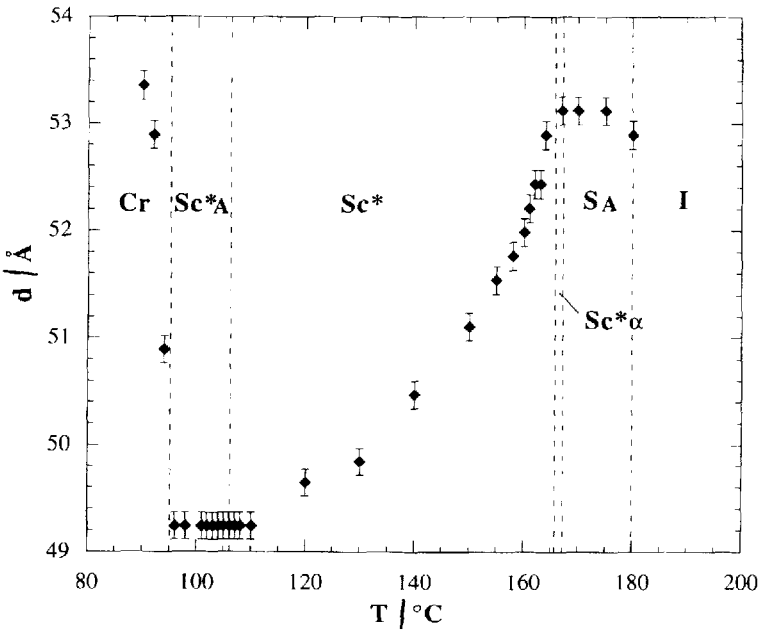

Figure 10. Temperature dependence of the layer spacing resulting from X-ray scans for 12BP5BBP8*, using a germanium monochromator (instrumental resolution: 7×10^{-3} Å^{-1}).

are plotted versus temperature. The parameters of the $S_{\tilde{C}*}$ phase are constant over its narrow range of existence. The 01 and 02 reflections of the $S_{\tilde{C}*}$ phase connect continuously to the first and second order reflections of the S_A phase. Moreover, concerning these two reflections, the pattern of oriented samples shows no difference between the $S_{\tilde{C}*}$ and the S_A phases. This seems to indicate that the director does not tilt with respect to the z-direction. But this interpretation does not exclude the occurrence of an $S_{\tilde{C}*}$ phase, since the average layer plane is no longer perpendicular to the director (the angle between the basic vectors a and c is equal to 108°). The schematic representation reported by Date *et al.* for their hexatic $S_{\tilde{C}}$ phase, figure 5(*b*) in [24], is consistent with our results. The transition from the S_A to the $S_{\tilde{C}*}$ phase could correspond to the formation of regular defects in the z-axis direction, but tilted from the layer plane due to the particular packing of the bent molecules.

Other compounds with an even number of methylene units have been studied only by optical microscopy and

Table 3. Transition temperatures (°C) and associated entropies ($\Delta S/R$) (in italics) resulting from DSC measurements and optical observations on the *m*BP*n*BBP8* series. ( ) denotes a monotropic transition; # is the sum of S_{C*}–$S_{C*\alpha}$ and $S_{C*\alpha}$–S_A entropies. The existence of an $S_{C*\alpha}$ phase is not always detected simply using only optical microscopy or DSC.

m	*n*	Cr		$S_{\tilde{C}*}$		S_{C*A}		S_{C*Fl}		S_{C*}		$S_{C*\alpha}$		S_A		I
8	5	• 150 *11·6*	—		•	(125·5)	•	(130·5)	•	(143·6) *0·005*	•	?	•	184·1 *3·6*	•	
8	6	• 115 *8·1*	•	132·3 *3·8*	—		—		—		—		—		•	
10	5	• 120 *11·4*			•	(112·6) *0·001*	•	(115·2) *0·005*	•	163·6 *0·063*	•	?	•	185·1 *4·3*	•	
10	6	• 104 *9·4*	•	131 *4·3*	—		—		—		—		—		•	
10	7	• 111 *9·7*			•	(105·8) *0·003*	•	(109·3) *0·005*	•	147·5 *0·1*	•	?	•	163·5 *4·8*	•	
10	8	• 98 *10·2*	•	122 *4·5*	—		—		—		—		—		•	
10	9	• 110 *11·2*	—		—		—		•	133 *0·09*	•	?	•	145·1 *4·8*	•	
12	5	• 95 *9·5*	—		•	106 *0·005*	•	106	•	162 *0·004*	•	?	•	180 *3·9*	•	
12	6	• 112 *20*	•	129·5 *4·4*	—		—		—		—		—		•	
16	5	• 100 *19·3*	—				—		•	176·2 *0·07*	•	?	•	180 *4·1*	•	
16	6	• 98 *18·4*	•	125·8 *1·5*	—		—		—		—		•	129 *2·6*	•	

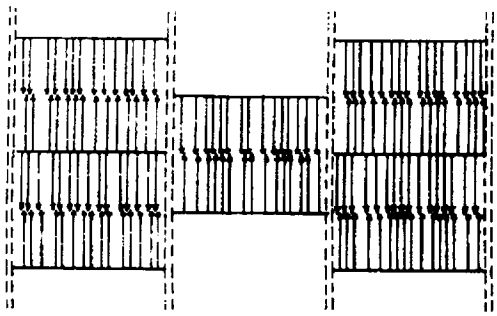

Figure 12. Real space representation for the fluid antiphase $S_{\tilde{A}}$ (centred rectangular structure).

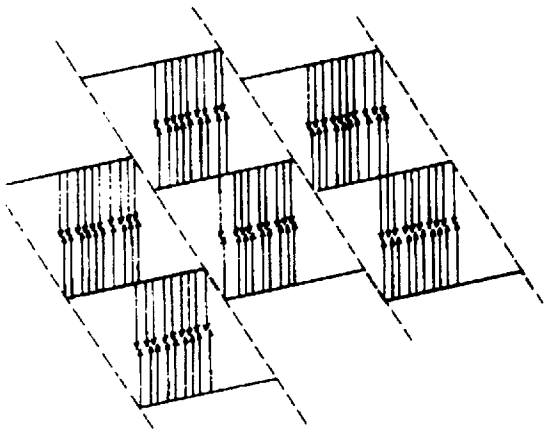

Figure 13. Real space representation for the ribbon phase $S_{\tilde{C}}$.

DSC. They display the same phases and their transition temperatures are reported in tables 3 and 4.

3.2. *The dependence of mesomorphic behaviour on alkoxy chain length*

3.2.1. *n is odd*

The effect of the alkoxy chain length was studied from $m=9$ to 16 for the series *m*BB5BBB8* (figure 17). The clearing temperatures regularly decrease with increasing *m*. The S_A and $S_{C*\alpha}$ ranges decrease, whereas the S_{C*} phase is stabilized. The $S_{C*\alpha}$ phase disappears from $m=13$. This behaviour is in complete agreement with results for benzoate esters containing three phenyl rings [13]. The transition temperatures of the *m*BP5BBP8* series confirm this tendency (see table 3).

3.2.2. *n is even*

Figure 18 shows the mesomorphic behaviour as a function of *m* (*m* ranging from 10 to 16) for the *m*BB6BBB8 series. The $S_{\tilde{C}*}$ phase exists for all the compounds over a wide enantiotropic temperature range

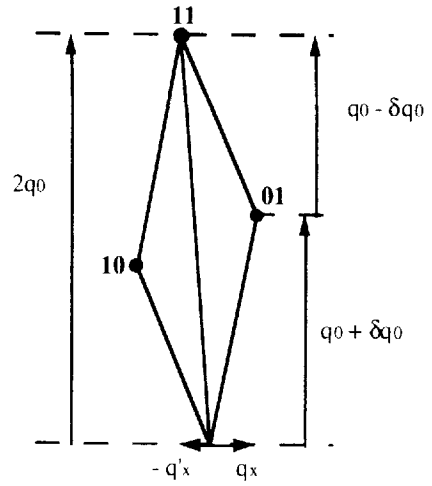

Figure 14. Possible two-dimensional matching of incommensurate wave vectors in the $S_{\tilde{C}}$ phase.

(between 19 and 48°C). From $m=10$ to 13, the clearing temperatures decrease with increasing m. Here, the direct transition from the $S_{\tilde{C}*}$ phase to the isotropic phase has a high associated entropy ($\Delta S/R=4{\cdot}7$). From $m=14$ to 16, an S_A phase is present at high temperatures. At the same time, the clearing temperatures cease to decrease with increasing m. The entropy change involved at the S_A I transition is much lower ($\Delta S/R=3{\cdot}5$) because the S_A phase is less ordered than the $S_{\tilde{C}*}$ phase.

A careful examination of table 3 shows that the other series behave in the same way.

3.3. *The dependence of mesomorphic behaviour on spacer length*

3.3.1. *n is odd*

The clearing temperatures reported in table 1 for th 10BB*n*BBB8* compounds ($n=3$ to 9) and table 3 fc the 10BP*n*BBP8* compounds ($n=5$ to 9) regularl decrease with increasing n. The longer spacers disfavou the existence of tilted phases. Increasing the spac length increases the molecular length, but also decoupl the interaction between the two mesogenic parts. Whe the spacer is short, the molecules behave as large lo molar mass compounds. Lengthening of the spacer ha not the same effect as lengthening of a terminal alkox chain. There, the modified parameter is the flexibility c the spacer.

3.3.2. *n is even*

Only three even values of n were examined ($n=4$, 8) for the 10BB*n*BBB8* series. They exhibit only a $S_{\tilde{C}*}$ phase and the clearing temperatures decreas monotonically.

3.3.3. *Odd–even effect of the number of methylene units*

Figure 19 summarizes the mesomorphic behaviour c the 10BB*n*BBB8* compounds. First of all, it is no clearly established that the mesomorphic sequenc depends on the parity of methylene units in the space the $S_{\tilde{C}*}$ phase exists when n is odd, whereas the variou S_{C*} phases are observed when n is even. The clearin temperatures are always higher in this latter case, an between two successive n-values of the spacer, the diffe

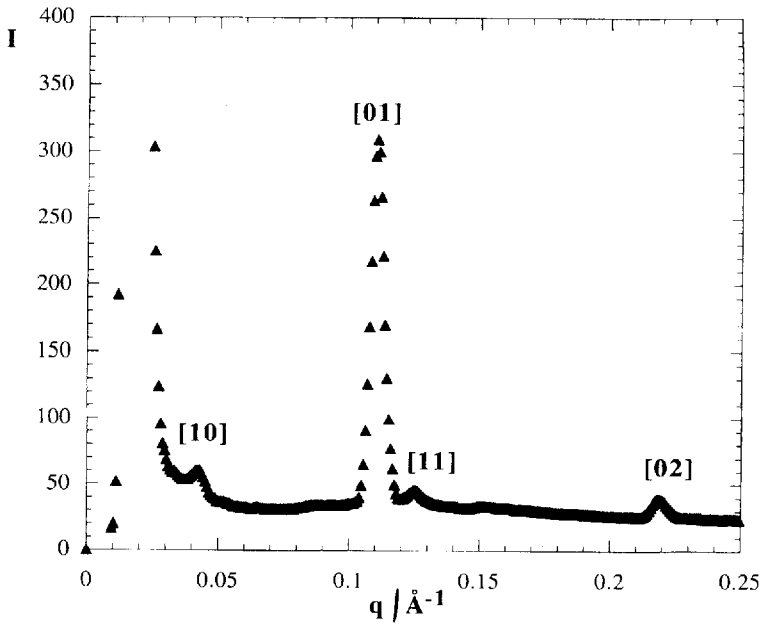

Figure 15. Intensity profile of the X-ray diffraction pattern of the $S_{\tilde{C}*}$ phase for 16BB6BBB8*.

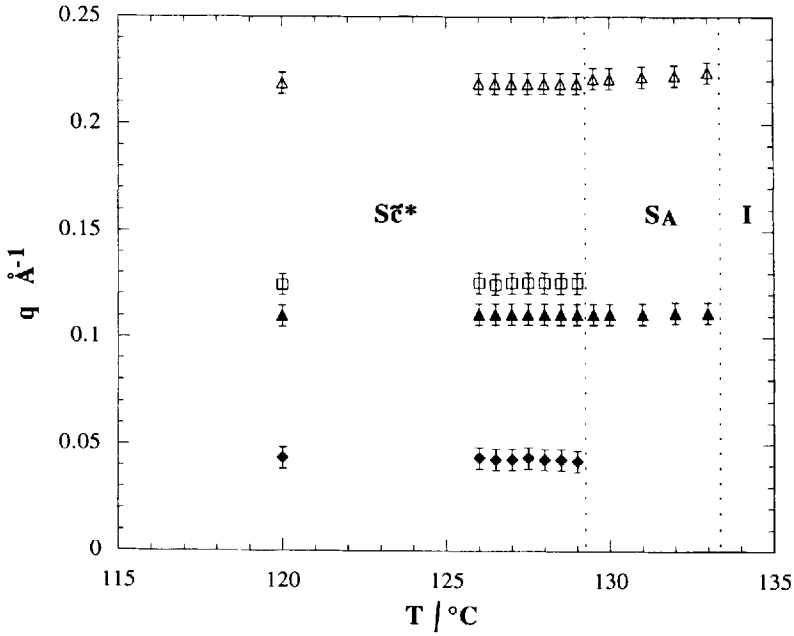

Figure 16. Temperature dependence of the wave vectors resulting from X-ray scans for 16BB6BBB8*, using a germanium monochromator (instrumental resolution: 7×10^{-3} Å^{-1}). Symbols: rhombis for q_1, triangles for q_2 (black for the first order, white for the second order), squares for q_3.

Table 4. Transition temperatures (°C) and associated entropies ($\Delta S/R$) (in italics) resulting from DSC measurements and optical observations on the *m*BB6BBB8* series. # denotes the sum of $S_{\tilde{c}*}$–S_A–I entropies.

m	*n*	Cr	$S_{\tilde{c}*}$	S_A	I
10	6	• 113	• 132	—	•
		13·8	*4·8*		
11	6	• 95	• 131	—	•
		14·3	*4·7*		
12	6	• 89	• 130·5	—	•
		17·5	*4·7*		
13	6	• 82	• 129·3	—	•
		15·7	*4·3*		
14	6	• 82	• 127·8	• 128·9	•
		15·1		*4·9#*	
15	6	• 84	• 126·5	• 130	•
		14·9	**0·8**	**2·3**	
16	6	• 87	• 127·6	• 132·6	•
		13·9	*0·9*	*2·7*	

ence can be more than 60°C. Furthermore, the entropy associated with the S_A–I transition exhibits an alternation depending on the parity of the spacer ($\Delta S/R = 4{\cdot}4$ for 16BB5BBB8* and 2·7 for 16BB6BBB8*). A strong alternation can also be noticed in the melting temperatures.

4. Discussion

The alternation of the mesomorphic behaviour with the parity of the spacer length indicates clearly the importance of the shape of the molecules. Indeed, when *n* is odd, the number of carbons in the spacer is even, because of the presence of a carboxy group; the molecules adopt a rod-like shape and behave like low molar mass compounds. When the number of carbons in the spacer is odd (*n* is even), the dimesogens have a bent average conformation. Then, the formation of a modulated phase is favoured.

The existence of such phases has been largely explained in terms of the existence of two competing periodicities for polar compounds, which were the first to display them. But modulated phases were also detected for non-polar polymeric mesogens [25, 26, 27], mesogens with fluorinated terminal chains [28, 29], and recently symmetric dimesogens [24]. The main feature of these latter systems is their strong steric asymmetry. Thus, two effects may be responsible for the existence of modulated phases: dipole–dipole interactions and steric repulsions. Of course, the distinction between these two effects is artificial since any steric difference between the head and tail of a compound also implies polarity. But we will distinguish the two cases and consider the prevailing effect.

Concerning chiral non-symmetric dimesogens, steric frustration must lead to the appearance of modulated phases. The $S_{\tilde{c}*}$ phase structural parameters are very similar to those obtained by Date *et al.* [24] with their symmetric dimers. The schematic model they suggested is also able to describe the microscopic arrangement in our system. The absence of any hexatic order in the $S_{\tilde{c}*}$ phase we have found could be explained in terms of the

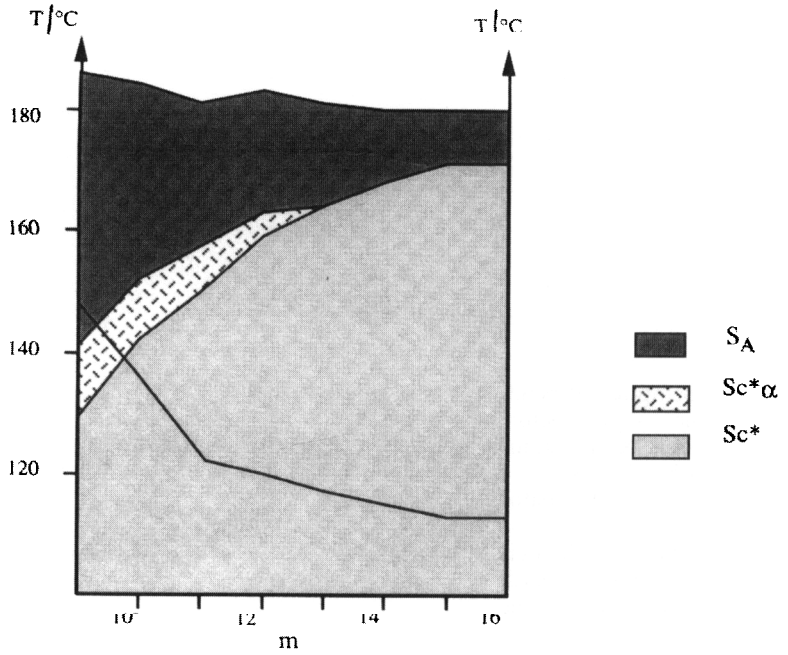

Figure 17. Mesomorphic behaviour versus number of carbon atoms (m) in the terminal alkoxy chain for the mBB5BBB8* series (even spacer).

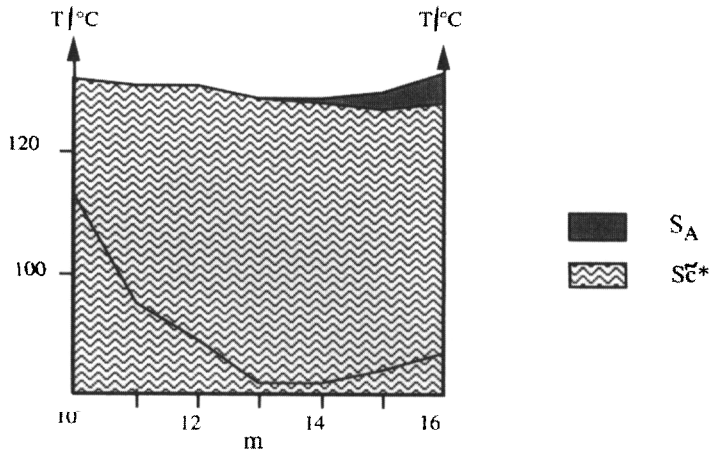

Figure 18. Mesomorphic behaviour versus number of carbon atoms (m) in the terminal alkoxy chain for the mBB6BBB8* series (odd spacer).

lack of a symmetry plane in our molecule due to the different length and nature of the two linked mesogens, and perhaps to the presence of a chiral centre. This probably rules out local order in the layer. Another interesting point is the stabilization of the S_A phase above the $S_{\tilde{C}*}$ phase when the length of the terminal chain increases. According to the proposed model, the chain is flexible enough to balance the bent shape of the molecule.

Another example of symmetric dimesogens involves the alternation of mesomorphic behaviour between odd and even spacers [30, 31]: an S_A phase exists for even members, whereas odd members form an S_{C2} phase, which has also been called S_{CA} since the tilt is opposite from one mesogen to the next. The periodicity of these dimers corresponds to half of the molecular length, indicating the intercalated nature of these smectic phases. It is worth noticing that modulated phases have always been observed in monolayered smectic systems.

For symmetric dimesogens, mesogen–mesogen interactions are the same for both intercalated and monolayer structures. Then, the terminal chain–spacer incompatibility is the factor responsible for any microphase separation. The layer ordering is related to the chemical structure, which governs the microscopic interactions. The following materials induce intercalated smectic phases [31]:

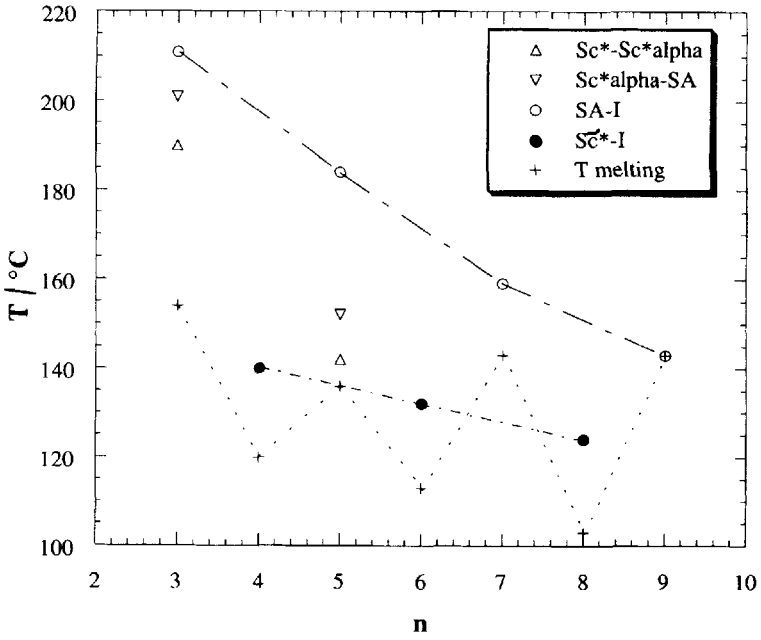

Figure 19. Dependence of the transition temperatures on the length of the spacer (n) for the 10BBnBBB8* series.

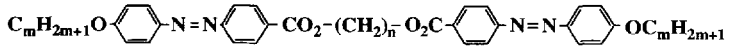

The dipole–dipole interaction between the central carboxy group and the ether group favours the intermolecular association of the terminal and spacer chains. On the contrary, the microphase separation observed for the compounds below [10], may be because of the absence of such dipole interactions:

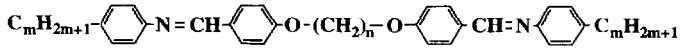

In our system, the different moieties also tend to segregate, but two effects can explain this phenomenon: the presence of two core lengths and the local polarity. Indeed, segregation may arise from the inability of two rigid moieties to pack together due to their different lengths, or from the chemical nature of the linking groups which do not favour the intermolecular association of the spacer and terminal chain. But we are not able at the moment to determine which effect prevails in determining the appearance of the monolayered smectic periodicity.

However, we are convinced that this type of layer ordering is responsible for the existence of the $S_{\tilde{C}*}$ phase and also of the various S_{C*} phases for even spacers. The S_{C*A} phase we have described above, must not be confused with the intercalated phase obtained in a dimer bearing two chiral centres on each side of the spacer [32]. The tilt varies from one layer to the next in each case. In a monolayer smectic order, two molecules are involved to form a basic pattern and the molecular interaction between layers could arise from the pairing of transverse dipole moments. When intercalation occurs, the antiparallel ordering between successive layers is forced to occur by the bent molecular shape [31, 32]. However, the S_{C2} phase was found not to be miscible with an S_{C*A} or S_{O*} phase despite their having similar layer thicknesses [33], and no tristable switching has been reported yet for the dimer possessing two chiral centres.

At this stage, many questions arise concerning the chemical parameters influencing the mesomorphic behaviour. We wonder especially why the mBBnBBB8* series does not favour the appearance of the antiferroelectric phase. A few other materials have been synthesized combining the different mesogenic parts previously used. Their mesomorphic behaviour is reported in table 5. We notice that the S_{C*A} phase is observed for those having a tolane or a biphenyl chiral mesogenic moiety, but not for a three ring dibenzoate core, whatever the short part to which it is linked. The three phenyl ring part seems to drive the antiferroelectric interactions.

The choice of the three phenyl ring moiety is the prevailing factor. Our earlier conclusions concerning the chemical parameters influencing the stability of the S_{C*A} phase still hold [13]. When the longitudinal dipolar moment is strong (as with a benzoate core), the S_A and S_{C*A} phases are stabilized and the S_{C*A} is not observed. Another important point is the choice of an appropriate chiral centre linked to the core by a strong dipolar moment. The replacement of the methyl group by an

Table 5. Transition temperatures (°C) for the following compounds:

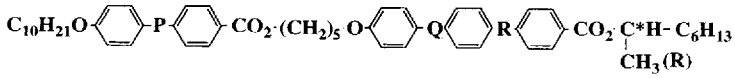

The existence of an $S_{C^*\alpha}$ phase is not always detected using only optical microscopy or DSC.

P	Q	R	Cr		S_{C^*A}		S_{C^*Fl}		S_{C^*}		$S_{C^*\alpha}$		S_A		I
CO_2	CO_2	CO_2	•	136	—		—		•	142·3	•	151·6	•	184·5	•
—	CO_2	CO_2	•	112	—		—		•	153	•	?	•	189	•
CO_2	C≡C	CO_2	•	106·2	•	(91)	•	(100)	•	154	•	157·6	•	186	•
—	C≡C	CO_2	•	131	•	(129·7)	•	133	•	171·5	•	174·4	•	193·8	•
CO_2	CO_2	—	•	111	•	(91)	•	(96)	•	142	•	?	•	178	•
—	CO_2	—	•	120	•	(111)	•	(115)	•	161	•	?	•	186	•

ethyl group on the asymmetric carbon enhances the S_{C^*A} phase [11, 20, 34].

The presence of a carboxy group between the short rigid core and the spacer also has a major effect on mesomorphic behaviour. Its replacement by an ether group cancels the existence of the S_{C^*A} and $S_{\tilde{C}^*}$ phases. Those results will be discussed in a forthcoming paper.

5. Conclusion

In this paper, we have described the synthesis of new examples of non-symmetric dimesogens. Their asymmetry comes from two structural factors: their rigid parts are different in length and only one of the two bears an asymmetric carbon. They display a rich variety of smectic phases, which are always organized in a monomolecular fashion. The spacer and tail groups tend to segregate into different regions. We cannot assess at the moment whether the driving force is favourable interactions between identical mesogenic parts or dipolar interactions associated with the different linking groups.

For such monolayered smectogenic systems, the odd–even alternation of the molecular shape with the number of carbons in the spacer induces two kinds of mesomorphic scenario:

(i) when the spacer is odd, the molecules are bent and the sequence is: $S_{\tilde{C}^*}$–S_A–I;

(ii) when the spacer is even, the molecules are of a rod-like conformation and the sequence is: S_{C^*A}–S_{C^*Fl}–S_{C^*}–$S_{C^*\alpha}$–S_A–I.

In this latter case, the dimesogens behave like low molar mass compounds. The stability of the S_{C^*A} phase depends mainly on the chiral mesogenic part, and depends on the same molecular influences as low molar mass AFLC.

Some further investigations are in progress to determine whether segregation results from the difference between the lengths of the mesogenic parts or from incompatibility of the spacer and tail moieties due to their lengths or the polarity of the linking groups.

6. Materials

6.1. *Synthesis of (R)-4-(1-methylheptyloxycarbonyl) phenyl 4-(4-benzyloxybenzoyloxy)benzoate* **7a**

To a solution of phenol **6a** [13] (2·96 g, 8 mmol) in CH_2Cl_2, were added DCC (1·8 g, 8·8 mmol), DMAP (0·09 g) and 4-benzyloxybenzoic acid (2 g, 8·8 mmol). The mixture was stirred at room temperature overnight, filtered and the solvent evaporated. The product was purified by chromatography on silica gel using CH_2Cl_2 as eluent and recrystallized from 95% ethanol. Yield: 2·95 g of ester, 65%, m.p. 152°C. ^{1}H NMR: δ(ppm): 0·9 (t, 3H, CH_3), 1·25 (m, 8H, 4 CH_2), 1·36 (d, 3H, CH_3–CH), 1·6–1·8 (m, 2H, CH_2–CHO), 5·2 (m, 3H, CH–O and CH_2–O), 7·1 (d, 2H arom), 7·3–7·5 (m, 9H arom), 8·2 (m, 4H arom), 8·3 (d, 2H arom). IR: 2918, 2848, 1703, 1601, 1250, 845, 773 cm^{-1}.

6.2. *Synthesis of (R) 4-(1-methylheptyloxycarbonyl) phenyl 4-(4-hydroxybenzoyloxy)benzoate* **8a**

The preceding ester **7a** was placed in 400 ml of ethyl acetate and 100 ml of 95% ethanol with palladium on carbon (0·2 g). Hydrogenolysis was carried out with heating. After filtration of the catalyst, the solvent was removed under low pressure and the phenol was recrystallized from a mixture of heptane and ethyl acetate (9 : 1). Yield: 2·4 g, 96%. ^{1}H NMR: δ(ppm): 0·9 (t, 3H, CH_3), 1·25 (m, 8H, 4 CH_2), 1·36 (d, 3H, CH_3–CH), 1·6–1·8 (m, 2H, CH_2–CHO), 5·2 (m, 1H, CH-O), 7·0 (d, 2H arom), 7·4 (m, 4H arom), 8·15 (m, 4H arom), 8·3 (d, 2H arom). IR: 3405, 2918, 2848, 1698, 1590, 1273, 845, 762 cm^{-1}.

6.3. *Synthesis of 4-(4-decyloxybenzoyloxy)benzoic acid* **12a**

The synthesis of the ester **11a** was realized following the procedure described in § 6.1. The product was recrystallized from 95% ethanol. Yield: 3·47 g of **11a**, 70%. The acid **12a** was obtained following the experimental route described in §6.2. Yield: 3·1 g of acid **12a**, 80%. Cr

131°C N > 250°C I. ^{1}H NMR: δ(ppm): 0·9 (t, 3H, CH_3), 1·3 (m, 12H, 6 CH_2), 1·5 (m, 2H, $CH_{2\gamma}$), 1·8 (m, 2H, $CH_{2\beta}$), 4·05 (t, 2H, CH_2–O), 7·0 (d, 2H arom), 7·4 (d, 2H arom), 8·2 (2d, 4H arom). IR: 3405, 2917, 2850, 1716, 1604, 1287, 1190, 833, 773 cm^{-1}.

6.4. *Synthesis of 5-hydroxypentyl 4-(4-decyloxybenzoyloxy)benzoate* **13a**

To a solution of 1,5-pentandiol (1·96 g, 0·02 mol) in CH_2Cl_2 (100 ml) were added DCC (1·13 g, 5·5 mmol) and DMAP (0·06 g). The acid **12a** (2 g, 5 mmol) was added progressively during 2 h. The mixture was stirred at room temperature overnight, filtered, the solvent evaporated and the product purified by chromatography on silica gel using a mixture of CH_2Cl_2 and ethyl acetate (95 : 5) as eluent. Yield: 0·525 g, 22%. Cr 80°C (S_C 77°C) I. ^{1}H NMR: δ(ppm): 0·9 (t, 3H, CH_3), 1·3–1·8 (m, 22H, 11 CH_2), 3·7 (t, 2H, CH_2O), 4·05 (t, 2H, CH_2–O), 4·2 (t, 2H, CH_2–O), 7·0 (d, 2H arom), 7·3 (d, 2H arom), 8·2 (2d, 4H arom). IR: 3360, 2914, 2825, 1730, 1710, 1608, 1282, 1069, 847, 763 cm^{-1}.

6.5. *Synthesis of (R)-4[4-(1-methylheptyloxycarbonyl) phenyloxycarbonyl]phenyl 4-{5-[4-(4-decyloxybenzoyloxy)benzoyloxy]pentyloxy}benzoate* (10BB5BBB8*)

The alcohol **13a** (0·24 g, 0·5 mmol), and the chiral phenol **8a** (0·25 g, 0·5 mmol) were placed in 10 ml of CH_2Cl_2 with DEAD (0·09 g, 0·5 mmol) and TPP (0·13 g, 0·5 mmol). This mixture was stirred at room temperature for 2 h. The solvent was evaporated under low pressure. The desired compound was purified by chromatography on silica gel using CH_2Cl_2 as eluent and recrystallized from absolute ethanol. Yield: 0·3 g, 60%. ^{1}H NMR: δ(ppm): 0·9 (t, 6H, 2 CH_3), 1·2–1·8 (m, 18 H, 9 CH_2), 3·6 (t, 2H, CH_2–O), 4·05–4·15 (m, 4H, 2 CH_2–O), 4·4 (t, 2H, O–CH_2), 5·15 (m, 1H, CH–CH_3), 7·0 (d, 4H arom), 7·4 (m, 8H arom), 8·1–8·3 (m, 8H arom). IR: 2918, 2850, 1730, 1698, 1604, 1290, 1190, 832, 771 cm^{-1}.

6.6. *Synthesis of ethyl 4-hydroxybiphenyl-4'-caroxylate* **2b**

In a 500 ml Erlenmeyer flask was placed the acid **1b** (10·5 g, 0·05 mol) in 150 ml of ethanol with 5 ml of H_2SO_4 and the mixture was stirred under reflux overnight. The solvent was evaporated and the solid treated with water. The organic phase was shaken with diethyl ether and washed three times with water. The product was purified by chromatography on silica gel using a mixture of toluene and ethyl acetate (8 : 2) as eluent. The ester was recristallized from absolute ethanol. Yield: 8·8 g of compound **2b**, 80%. Cr_1 134°C Cr_2 142°C I. ^{1}H NMR: δ(ppm): 1·4 (t, 3H, CH_3), 4·4 (q, 2H, CH_2–O), 6·95 (d, 2H arom), 7·6 (2d, 4H arom), 8,1 (d, 2H arom). IR: 3334, 2914, 2825, 1680, 1601, 1586, 1279, 1192, 833, 774 cm^{-1}.

6.7. *Synthesis of 4-(4-benzyloxy)biphenyl-4'-carboxylic acid* **3b**

In an Erlenmeyer flask was introduced the ester **2b** (8·5 g, 0·035 mol) in 150 ml of ethanol with potassium hydroxyde (2·15 g). The solution was heated under reflux and a solution of benzyl bromide (6·3 g, 0·037 mol) in 10 ml of ethanol was added dropwise. The reaction mixture was stirred under reflux for 4 h. Afterwards, it was saponified with sodium hydroxyde (5·6 g, 0·1 mol) in 10 ml of water under reflux. Addition of 13 ml of concentrated hydrochloric acid gave the acid which was filtered off, washed with water and recrystallized from 800 ml of glacial acetic acid. Yield: 9·5 g of acid **3b**, 90%, m.p. 270°C. IR: 3360, 1680, 1432, 1273, 1258, 834, 773 cm^{-1}.

6.8. *Synthesis of (R)-1-methylheptyl 4-(4-benzyloxy) biphenyl-4'-carboxylate* **4b**

A solution of 300 ml of toluene containing oxalyl chloride and carboxylic acid **3b** (9·12 g, 0·03 mol) was heated under reflux for 2 h. After the solvent had been removed under reduced pressure, the acid chloride solution in CH_2Cl_2 was added dropwise to a mixture of (*R*)-2-octanol (3·9 g, 0·03 mol) in 150 ml of CH_2Cl_2 and 25 ml of pyridine. This was stirred for three days and treated with 50 ml of hydrochloric acid (1M). The product was filtered off, washed and recrystallized from 95% ethanol. Yield: 8·6 g of compound **4b**, 70%, m.p. 105°C. ^{1}H NMR: δ(ppm): 0·9 (t, 3H, CH_3), 1·25 (m, 8H, 4 CH_2), 1·35 (d, 3H, CH_3–CH), 1·6–1·8 (m, 2H, CH_2–CHO), 5·15 (s, 2H, CH_2–O), 5·2 (m, 1H, CH–O), 7·1 (d, 2H arom), 7·4 (m, 4H arom), 7·6 (m, 5H arom), 8·05 (d, 2H arom). IR: 2918, 2848, 1703, 1601, 1294, 1200, 831, 773 cm^{-1}.

6.9. *Synthesis of (R)-1-methylheptyl 4-hydroxybiphenyl-4'-carboxylate* **5b**

The phenol **5b** was obtained following the experimental procedure described in §6.2. The solid was recrystallized from a mixture of ethyl acetate and heptane (1 : 9). Yield: 7·3 g of **5b**, 79%, m.p. 86°C. ^{1}H NMR: δ(ppm): 0·9 (t, 3H, CH_3), 1·25 (m, 8H, 4 CH_2), 1·35 (d, 3H, CH_3–CH), 1·6–1·8 (m, 2H, CH_2–CHO), 5·2 (m, 1H, CH–O), 7·0 (d, 2H arom), 7·6 (2d, 4H arom), 8·1 (d, 2H arom). IR: 3354, 2918, 1684, 1601, 1588, 1295, 1276, 1197, 834, 773 cm^{-1}.

6.10. *Synthesis of (R)-1-methylheptyl 4-(4-benzyloxybenzoyloxy)biphenyl-4'-carboxylate* **6b**

The ester **6b** was synthesized following the experimental procedure described in §6.1. Yield: 2·2 g of ester **6b**, 80%, m.p. 116°C. ^{1}H NMR: δ(ppm): 0·9 (t, 3H, CH_3),

1·25 (m, 8H, 4 CH_2), 1·35 (d, 3H, CH3–CH), 1·6–1·8 (m, 2H, CH_2–CHO), 5·2 (m, 3H, CH–O and CH_2–O), 7·1 (d, 2H arom), 7·4–7·6 (m, 7H arom), 7·65 (d, 4H arom), 8·2 (2d, 4H arom). IR: 2918, 2848, 1684, 1601, 1588, 1295, 1276, 1197, 834, 775 cm^{-1}.

6.11. *Synthesis of (R)-1-methylheptyl 4-(4-hydroxybenzoyloxy)biphenyl-4'-carboxylate* **7b**

This compound was obtained following the synthetic route used for **5b**. Yield: 1·7 g of chiral phenol **7b**, 92%, m.p. 156°C. ^1H NMR: δ(ppm): 0·9 (t, 3H, CH_3), 1·25 (m, 8H, 4 CH_2), 1·35 (d, 3H, CH_3–CH), 1·6–1·8 (m, 2H, CH_2–CHO), 5·2 (m, 3H, CH–O and CH_2–O), 6·95 (d, 2H arom), 7·3 (d, 2H arom), 7·7 (2d, 4H arom), 8·2 (2d, 4H arom). IR: 3409, 2918, 2848, 1702, 1602, 1586, 1276, 1190, 890, 773 cm^{-1}.

6.12. *Synthesis of 4-octyloxybiphenyl-4'-carboxylic acid* **8b** [35]

A mixture of 100 ml of ethanol with potassium hydroxyde (2 g, 0·035 mol) and 4-hydroxybiphenyl-4'-carboxylic acid **2b** (5 g, 0·023 mol) was heated at 80°C. A solution of 1-bromo-octane (5·8 g, 0·03 mol) in 30 ml of ethanol was added dropwise and the reaction continued under reflux for 4 h. After cooling to room temperature, potassium hydroxide (3 g) was added. Further heating under reflux for 2 h was followed by cooling in an ice bath and hydrolysis with hydrochloric acid. The precipitate was filtered off, washed with water and recrystallized from 200 ml of pure acetic acid. Yield: 6·5 g, 80%. Cr 183°C S_C 255°C N 264°C I. IR: 3360, 2917, 2848, 1685, 1604, 1276, 837, 771 cm^{-1}.

6.13. *Synthesis of 6-benzyloxyhexyl 4-octyloxybiphenyl-4'-carboxylate* **11b**

In an Erlenmeyer flask containing 50 ml of toluene were placed 1,6-hexandiol (6·2 g, 0·06 mol) and sodium pieces (1·38 g, 0·06 mol). This mixture was heated at 80°C for 2 h and maintained at 60°C overnight. It was then heated under reflux and a solution of benzyl bromide (9·3 g, 0·054 mol) in 30 ml of toluene was added dropwise. The reaction was continued at this temperature for 3 h. Then, it was cooled down to 0°C and treated with hydrochloric acid (1 M). The reaction mixture was poured into water and extracted with diethyl ether. The organic phase was washed with water and dried over anhydrous sodium sulphate; the solvent was removed under reduced pressure. The yield was 8·8 g of nearly pure product **10b**.

The liquid containing mainly 6-benzyloxyhexan-1-ol (1 g, ~5·5 mmol) was placed in 25 ml of CH_2Cl_2 with 4-octyloxybiphenyl-4'-carboxylic acid (5 mmol), DCC (1·1 g, 5·5 mmol) and DMAP (0·1 g). This mixture was stirred at room temperature overnight. It was then filtered and the solvent evaporated. The ester was purified by chromatography on silica gel using a mixture of heptane and ethyl acetate (75:25) as eluent and recrystallized from 95% ethanol. Yield: 1·8 g, 70%. Cr 38°C S_A 42°C I. ^1H NMR ($CDCl_3$): δ(ppm): 0·9 (t, 3H, CH_3), 1·2–1·8 (m, 18 H, 9 CH_2), 3·5 (t, 2H, CH_2–O), 4 (t, 2H, CO_2–CH_2), 4·35 (t, 2H, CH_2–O), 4·55 (s, 2H, CH_2–O–Ph), 7 (d, 2H arom), 7·3 (m, 5H arom), 7·6 (2d, 4H arom), 8·1 (d, 2H arom). IR: 2917, 2850, 1716, 1604, 1287, 1199, 1113, 831, 770 cm^{-1}.

6.14. *Synthesis of 6-hydroxyhexyl 4-octyloxybiphenyl-4'-carboxylate* **12b**

To a mixture of ethyl acetate (20 ml) and 95% ethanol (1·5 ml) were added **11b** (1·8 g, 3 mmol), palladium dihydroxide (0·1 g) and cyclohexene (4·5 ml). The reaction mixture was heated at reflux under nitrogen for at least 2 h. If the hydrogenolysis was not complete, the same amounts of $Pd(OH)_2$ and cyclohexene were added again. The catalyst was filtered off and the solvent evaporated under vacuum. The product was purified on silica gel using CH_2Cl_2 and ethyl acetate as eluent and recrystallized from a mixture of heptane and ethyl acetate (9:1). Yield: 1·4 g, 90%. Cr 90°C S_A 96°C I. ^1H NMR ($CDCl_3$): δ(ppm): 0·9 (t, 3H, CH_3), 1·2–1·8 (m, 18 H, 9 CH_2), 3·6 (t, 2H, CH_2–O), 3·95 (t, 2H, CO_2–CH_2), 4·25 (t, 2H, CH_2–OH), 6·95 (d, 2H arom), 7·55 (2d, 4H arom), 8 (d, 2H arom). IR: 3360, 2918, 2871, 1716, 1604, 1295, 1272, 1190, 832, 768 cm^{-1}.

6.15. *Synthesis of (R)-4-(1-methylheptyloxycarbonyl)]biphenyl-4'-yl 4-(6-[4-octyloxybiphenyl-4'-carbonyloxy]hexyloxy)benzoate* (8BP6BBP8*)

The alcohol **12b** (0·213 g, 0·5 mmol) and the chiral phenol **7b** (0·223 g, 0·5 mmol) were placed in 10 ml of CH_2Cl_2 with diethyl azodicarboxylate (DEAD) (0·09 g, 0·5 mmol) and triphenylphosphine (TPP) (0·131 g, 0·5 mmol). This mixture was stirred at room temperature for 2 h. The solvent was evaporated under low pressure. The residue was purified by chromatography on silica gel using CH_2Cl_2 as eluent and recrystallized from absolute ethanol. Yield: 0·2 g, 50%. ^1H NMR: δ(ppm): 0·9 (t, 6H, 2CH_3), 1·2–1·9 (m, 37 H, CH_3–CH, 17 CH_2), 4·05 (t, 2H, CH_2–O), 4·35 (t, 2H, CH_2–O), 5·15 (m, 1H, CH–CH_3), 6·95 (2d, 4H arom), 7·2 (d, 2H arom), 7·6 (m, 8H arom), 8·15 (m, 6H arom). IR: 2919, 2850, 1729, 1711, 1604, 1288, 1189, 1110, 829, 772 cm^{-1}.

The authors are very grateful to G. Sigaud, M.F. Achard and F. Hardouin for their fruitful suggestions. They also wish to thank the G.D.R. 'Cristaux Liquides Ferroélectriques' for its financial support.

References

[1] GRIFFIN, A. C., and BRITT, T. R., 1981, *J. Am. chem. Soc.*, **103,** 4957.

[2] HARDOUIN, F., RICHARD, H., and ACHARD, M. F., 1993, *Liq. Cryst.*, **14,** 971.

[3] (*a*)EMSLEY, J. W., LUCKHURST, G. R., SHILSTON, G. N., and SAGE, I., 1984, *Mol. Cryst. liq. Cryst. Lett.*, **102,** 223; (*b*)IMRIE, C. T., 1989, *Liq. Cryst.*, **6,** 391.

[4] GRIFFIN, A. C., and VAIDYA, S. R., 1988, *Liq. Cryst.*, **3,** 1275.

[5] ATTARD, G. S., DATE, R. W., IMRIE, C. T., LUCKHURST, G. R., ROSKILLY, S. J., SEDDON, J. M., and TAYLOR, L., 1994, *Liq. Cryst.*, **16,** 529.

[6] HARDOUIN, F., ACHARD, M. F., JIN, J. I., SHIN, J. W., and YUN, Y. K., 1994, *J. Phys. II*, **4,** 627.

[7] FERRARINI, A., LUCKHURST, G. R., NORDIO, P. L., and ROSKILLY, S. J., 1994, *J. chem. Phys.*, **2,** 100.

[8] HARDOUIN, F., ACHARD, M. F., JIN, J. I., and YUN, Y. K., 1995, *J. Phys. II*, **5,** 927.

[9] BLATCH, A. E., FLETCHER, I. D., and LUCKHURST, G. R., 1995, *Liq. Cryst.*, **18,** 801.

[10] DATE, R. W., IMRIE, C. T., LUCKHURST, G. R., and SEDDON, J. M., 1992, *Liq. Cryst.*, **12,** 203.

[11] FAYE, V., NGUYEN, H. T., LAUX, V., and ISAERT, N., *Ferroelectrics*, (in the press).

[12] GOODBY, J. W., PATEL, J. S., and CHIN, E., 1992, *J. Mater. Chem.*, **2,** 197.

[13] FAYE, V., ROUILLON, J. C., DESTRADE, C., and NGUYEN, H. T., 1995, *Liq. Cryst.*, **19,** 47.

[14] BRUNET, M., and ISAERT, N., 1988, *Ferroelectrics*, **84,** 25.

[15] NGUYEN, H. T., ROUILLON, J. C., CLUZEAU, P., SIGAUD, G., DESTRADE, C., and ISAERT, N., 1994, *Liq. Cryst.*, **17,** 571.

[16] LAUX, V., ISAERT, N., NGUYEN, H. T., CLUZEAU, P., and DESTRADE, C., 1995, in Proceedings of *5th Int. Conf. Ferro. L. C., Cambridge*, p35.

[17] DUPONT, L., GLOGAROVA, M., MARCEROU, J. P., NGUYEN, H. T., and DESTRADE, C., 1991, *J. Phys. II*, **1,** 831.

[18] ZAREBA, I., ALLOUCHI, H., COTRAIT, M., DESTRADE, C., and NGUYEN, H. T., 1996, *Acta Cryst.*, **C52,** 441.

[19] HORI, K., and ENDO, K., 1993, *Bull. chem. Soc. Jpn.*, **66,** 46.

[20] OUCHI, Y., YOSHIOKA, Y., ISHII, H., SEKI, K., KITAMURA, M., NOYORI, R., TAKANISHI, Y., and NISHIYAMA, I., 1995, *J. Mater. Chem.*, **5,** 2297.

[21] HARDOUIN, F., NGUYEN, H. T., ACHARD, M. F., and LEVELUT, A. M., 1982, *J. Phys. Lett.*, **43,** 327.

[22] HARDOUIN, F., LEVELUT, A. M., ACHARD, M. F., and SIGAUD, G., 1983, *J. Chim. Phys.*, **80,** 53.

[23] SIGAUD, G., HARDOUIN, F., ACHARD, M. F., and LEVELUT, A. M., 1981, *J. Phys.*, **42,** 107.

[24] DATE, R. W., LUCKHURST, G. R., SHUMAN, M., and SEDDON, J. M., 1995, *J. Phys. II*, **5,** 587.

[25] WATANABE, J., NAKATA, Y., and SIMIZU, K., 1994, *J. Phys. II*, **4,** 581.

[26] DAVIDSON, P., KELLER, P., and LEVELUT, A. M., 1985, *J. Phys.*, **46,** 939.

[27] ENDRES, B. W., EBERT, M., WENDORFF, J. H., RECK, B., and RINGSDORF, H., 1990, *Liq. Cryst.*, **7,** 217.

[28] LOBKO, T. A., and OSTROVSKII, B. I., 1992, *Mol. Mater.*, **1,** 99.

[29] NGUYEN, H. T., SIGAUD, G., ACHARD, M. F., HARDOUIN, F., TWIEG, R. J., and BETTERTON, K., 1991, *Liq. Cryst.*, **10,** 389.

[30] WATANABE, T., KOMURA, H., and NIORI, T., 1993, *Liq. Cryst.*, **13,** 455.

[31] NIORI, T., ADACHI, S., and WATANABE, J., 1995, *Liq. Cryst.*, **19,** 139.

[32] HASHIMOTO, S., ISOZAKI, T., SUZUKI, Y., KUSUMOTO, T., HIYAMA, T., TAKANISHI, Y., TAKEZOE, H., and FUKUDA, A., 1995, in Proceedings of *5th Int. Conf. Ferro. L. C., Cambridge*, p33.

[33] TAKANISHI, Y., TAKEZOE, H., JOHNO, M., YUI, T., and FUKUDA, A., 1993, *Jpn. J. appl. Phys.*, **32,** 4605.

[34] NISHIYAMA, I., and GOODBY, J. W., 1993, *J. Mater. Chem.*, **3,** 149.

[35] GRAY, G. W., HARTLEY, J. B., and JONES, B., 1955, *J. chem. Soc.*, 1412.